

Increased fatty acid metabolism and decreased glycolysis are hallmarks of metabolic reprogramming within microglia in degenerating white matter during recovery from experimental stroke

Journal of Cerebral Blood Flow & Metabolism
2023, Vol. 43(7) 1099–1114
© The Author(s) 2023



Article reuse guidelines:
sagepub.com/journals-permissions
DOI: 10.1177/0271678X231157298
journals.sagepub.com/home/jcbfm



Sanna H Loppi¹ , Marco A Tavera-Garcia¹,
Danielle A Becktel¹ , Boaz K Maiyo¹, Kristos E Johnson¹,
Thuy-Vi V Nguyen², Rick G Schnellmann^{3,4} and
Kristian P Doyle^{1,2,4,5,6,7}

Abstract

The goal of this study was to evaluate changes in metabolic homeostasis during the first 12 weeks of recovery in a distal middle cerebral artery occlusion mouse model of stroke. To achieve this goal, we compared the brain metabolomes of ipsilateral and contralateral hemispheres from aged male mice up to 12 weeks after stroke to that of age-matched naïve and sham mice. There were 707 biochemicals detected in each sample by liquid chromatography-mass spectroscopy (LC-MS). Mitochondrial fatty acid β -oxidation, indicated by acyl carnitine levels, was increased in stroked tissue at 1 day and 4 weeks following stroke. Glucose and several glycolytic intermediates were elevated in the ipsilateral hemisphere for 12 weeks compared to the aged naïve controls, but pyruvate was decreased. Additionally, itaconate, a glycolysis inhibitor associated with activation of anti-inflammatory mechanisms in myeloid cells, was higher in the same comparisons. Spatial transcriptomics and RNA in situ hybridization localized these alterations to microglia within the area of axonal degeneration. These results indicate that chronic metabolic differences exist between stroked and control brains, including alterations in fatty acid metabolism and glycolysis within microglia in areas of degenerating white matter for at least 12 weeks after stroke.

Keywords

β -Oxidation, glycolysis, itaconate, metabolism, stroke

Received 6 October 2022; Revised 22 December 2022; Accepted 20 January 2023

¹Department of Immunobiology, College of Medicine, University of Arizona, Tucson, Arizona, USA

²Department of Neurology, College of Medicine, University of Arizona, Tucson, Arizona, USA

³Department of Pharmacology and Toxicology, College of Pharmacy, University of Arizona, Tucson, Arizona, USA

⁴BIO5 Institute, College of Medicine, University of Arizona, Tucson, Arizona, USA

⁵Arizona Center on Aging, College of Medicine, University of Arizona, Tucson, Arizona, USA

⁶Department of Psychology, College of Medicine, University of Arizona, Tucson, Arizona, USA

⁷Department of Neurosurgery, College of Medicine, University of Arizona, Tucson, Arizona, USA

Corresponding author:

Kristian P Doyle, Department of Immunobiology, University of Arizona, 1656 E. Mabel Street, P.O. Box 245221, Tucson, Arizona 85719, USA.
Email: doylekr@arizona.edu

Introduction

Stroke is among the leading causes of death and disability, and markedly diminishes the quality of life of stroke survivors.¹ While mechanical thrombectomy can be used to treat large vessel occlusions in the anterior circulation,² recombinant tissue plasminogen activator (r-tPA) remains the only clinically approved pharmacological treatment for ischemic stroke. However, r-tPA is only suitable for a fraction of patients due to its narrow therapeutic time window and side effects.³ There is an urgent need to identify new targets for improving stroke recovery.

Ischemic strokes are caused by the blockage or narrowing of a brain blood vessel which results in insufficient delivery of oxygen and glucose to support cellular homeostasis. Although this acute perturbation in brain metabolism is well characterized, little is known about how brain metabolism is altered in the weeks and months during recovery. This is an important knowledge gap to address because, although cells adapt to their environment by undergoing metabolic reprogramming, metabolic reprogramming also alters cellular function.⁴ Therefore, knowing more about metabolic changes in the brain in the chronic period after stroke may reveal new targets for intervention. Furthermore, long-lasting metabolic abnormalities in the brain may be amenable for diagnostic neuroimaging.

Accordingly, the goal of this study was to evaluate how metabolism is altered in the brain in the first 12 weeks after stroke, which is when most recovery takes place.⁵ To accomplish this goal, we performed liquid chromatography-mass spectroscopy (LC-MS) global metabolomics on brain tissue from 7 month and 18- to 20-month-old C57BL/6J mice to determine how aging impacts brain metabolism as most strokes occur in people over the age of 65.⁶

We then performed LC-MS global metabolomics on the contralateral and ipsilateral hemispheres with the infarcts removed of 18 to 20-month-old mice sacrificed at 1 day and 2, 4, 8 and 12 weeks after stroke or sham surgery to evaluate how stroke impacts brain metabolism during recovery. Spatial transcriptomics and RNA *in situ*-hybridization were then conducted at 4 weeks post stroke to localize the metabolomic findings to particular brain areas and specific cell types.

Material and methods

Animals

Sample sizes for the study were determined using power calculation with G*Power software (version 3.1.9.7, Heinrich Heine Universität, Düsseldorf, Germany;

downloaded from <https://www.psychologie.hhu.de/arbeitsgruppen/allgemeine-psychologie-und-arbeitspsychologie/gpower.html>).⁷ With an effect size (based on estimated group means and standard deviations (SDs) from previous experiments) of 2.5, α 0.05 and power 90%, the group size was determined to be 5. Due to stroke surgery causing increased mortality in aged animals, group sizes were increased by 1–2 animals as necessary, to ensure that the final n would be 5 in each group. In total, 86 male C57BL/6J mice, sourced from the aged rodent colony at the National Institute on Aging, were used in this study. Six of them were young adults (7-month-old), and 80 were aged (18 to 20-month-old). The young mice were sacrificed without undergoing stroke or sham surgery (young naïve group). Four of the aged mice were stroked and sacrificed at 4 weeks post stroke for spatial transcriptomics and RNA *in situ*-hybridization. The remaining 76 mice were divided randomly (using GraphPad Prism Quick Calcs) into the following three groups: aged naïve ($n=6$), aged sham ($n=30$), and aged stroke ($n=40$). The aged stroke and sham mice were sacrificed at 1 day post ischemia (dpi) (7 stroke and 6 sham) and 2 weeks (7 stroke and 6 sham), 4 weeks (7 stroke and 6 sham), 8 weeks (6 stroke and 6 sham), and 12 weeks (6 stroke and 6 sham) after stroke or sham surgery (Figure 1(a)). The pre-set exclusion criteria of the study were (1) unsuccessful induction of ischemia (4 mice), (2) death of the animal during the experiment (3 mice), and (3) being a statistically significant outlier in any of the analyses (4 mice). All animal experiments followed the NIH guidelines and were approved by the University of Arizona Institutional Animal Care and Use Committee. RIGOR criteria and ARRIVE guidelines were followed when conducting and reporting the experiments.^{8,9} Every effort was made to minimize the harm and suffering of the animals.

Stroke and sham surgeries

The permanent distal middle cerebral artery occlusion (dMCAO) was carried out as described previously.¹⁰ Briefly, anesthesia was induced with 3% isoflurane (JD Medical, Phoenix, AZ, USA), and maintained throughout surgery. After the temporalis muscle was exposed and retracted, a hole (1 mm in diameter) was drilled into the temporal bone to expose the MCA. The dura was removed, after which the artery was cauterized. The temporalis muscle was replaced, and the wound closed using surgical glue. Body temperature of the animals was maintained at $37 \pm 0.5^\circ\text{C}$ during the procedure using a heating pad equipped with a rectal probe. Respiration and temperature were monitored throughout surgery. Immediately after surgery,

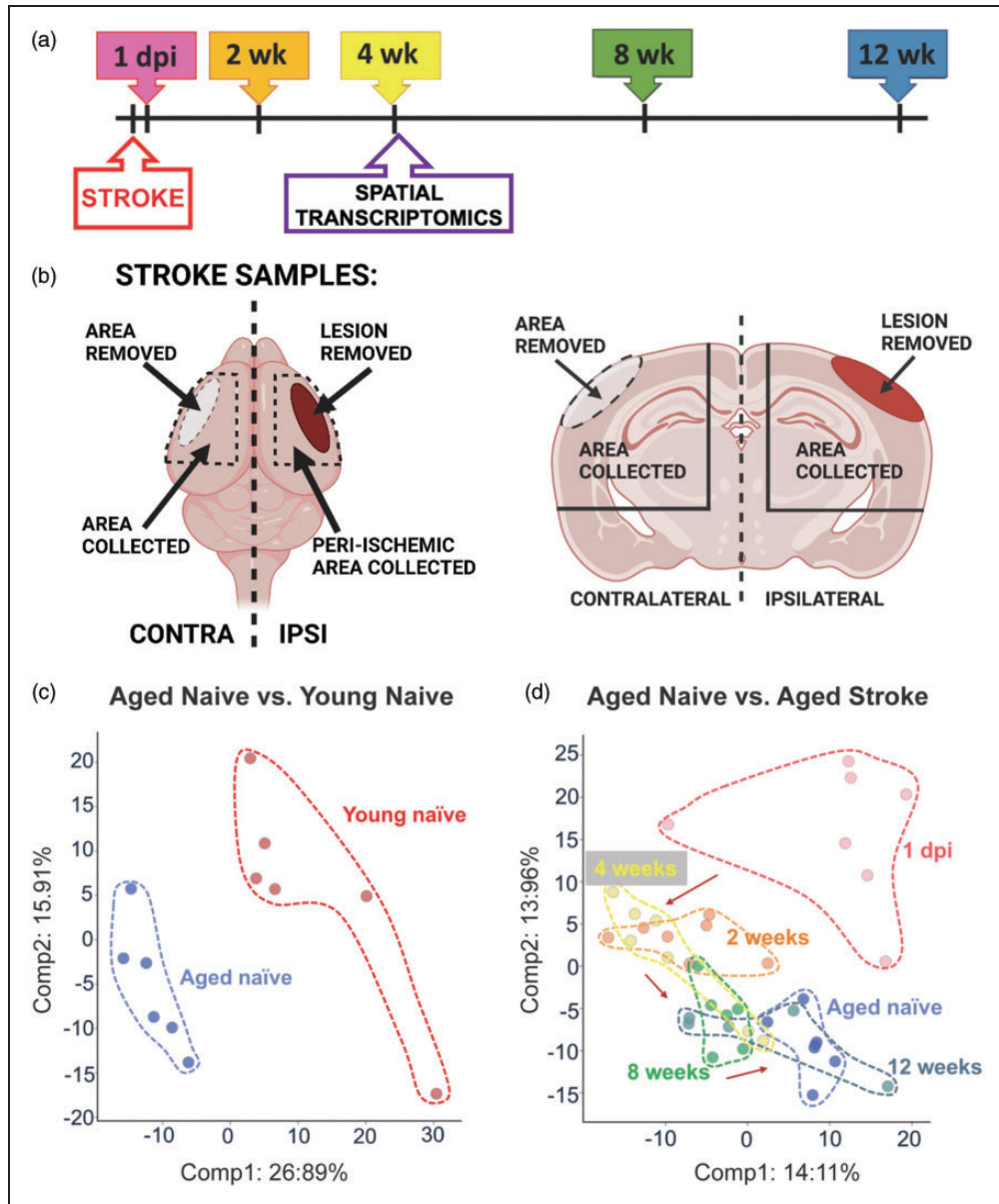


Figure 1. Study design and principal component analysis (PCA). (a) Timeline indicating the time points of tissue collection after stroke or sham surgery. (b) Schematic illustration of the locations where the samples were collected. (c) PCA showing a clear separation between the young and the aged naïve mice along Principal Component 1 and (d) PCA between the aged naïve mice and the stroke groups showing separation based on stroke time point.

mice were placed in a hypoxia chamber (Coy Laboratory products, Grass Lake, MI, USA) containing 9% oxygen and 91% nitrogen for 45 minutes. The purpose of hypoxia in this model is to both increase infarct size and reduce variability in infarct size.¹⁰ A single dose of buprenorphine hydrochloride (Buprenex[®] Injection 0.3 mg/mL, Henry Schein Medical, Melville, NY, USA; 0.1 mg/kg s.c.) was administered prior to surgery, and sustained release buprenorphine (Buprenorphine SR 1 mg/mL, Zoopharm LLC,

Laramie, WY, USA; 1 mg/kg s.c.) was administered 24 hours after surgery as a post-operative analgesic. The same steps, including 45 minutes of hypoxia, were performed on sham operated animals, except for cauterizing the MCA.

Perfusion and tissue collection

At the time points described in Figure 1(a), mice were anesthetized with 3% isoflurane. Blood samples were

collected from the heart, after which mice were transcardially perfused with 0.9% saline solution. For the spatial transcriptomics and RNA *in situ*-hybridization, whole brains were carefully removed and placed immediately into 4% PFA in PBS for 22 hours at 4°C, after which they were transferred to 30% sucrose solution at 4°C for 48 hours, embedded in paraffin, and cut into 7 µm thick sections. For the rest of the mice, infarcts and the corresponding regions from sham operated mice were dissected and removed. The infarcts generated by this permanent ischemia model can be easily identified and removed due to their cortical location and distinctive pallor and texture. The corresponding areas of the contralateral hemisphere were also dissected and removed. After removal of the olfactory bulb and cerebellum, the remaining ipsilateral and contralateral hemispheres were snap frozen in liquid nitrogen and shipped to Metabolon Inc. (Morrisville, NC, USA) for metabolomic analysis. The tissue was not further separated into smaller brain regions due to a minimum requirement of 50 mg of tissue outlined in Metabolon's global metabolic profiling protocol. A guide to the dissection is provided in Figure 1(b).

Metabolomic analysis

Global metabolite profiling analysis on brain tissue was performed by Metabolon Inc. using ultra high-performance liquid chromatography coupled to tandem mass spectrometry (UPLC-MS/MS). In brief, following receipt by Metabolon, samples were inventoried and immediately stored at -80°C. Samples were prepared using the automated MicroLab STAR[®] system from Hamilton Company (Reno, NV/Franklin, MA, USA). Several recovery standards were added prior to the first step in the extraction process for quality control (QC) purposes. To remove protein, dissociated small molecules bound to protein or trapped in the precipitated protein matrix, and to recover chemically diverse metabolites, proteins were precipitated with methanol under vigorous shaking for 2 min (GenoGrinder 2000; Glen Mills, Clifton, NJ, USA) followed by centrifugation. The resulting extract was divided into five fractions: two for analysis by two separate reverse phase (RP)/UPLC-MS/MS methods with positive ion mode electrospray ionization (ESI), one for analysis by RP/UPLC-MS/MS with negative ion mode ESI, one for analysis by HILIC/UPLC-MS/MS with negative ion mode ESI, and one reserved for backup. Samples were placed briefly on a TurboVap[®] (Zymark, Biotage, Uppsala, Sweden) to remove the organic solvent. The sample extracts were stored overnight under nitrogen before preparation for analysis.

Several types of controls were analyzed in concert with the experimental samples: a pooled matrix sample generated by taking a small volume of each experimental sample served as a technical replicate throughout the data set; extracted water samples served as process blanks; and a cocktail of QC standards that were carefully chosen not to interfere with the measurement of endogenous compounds were spiked into every analyzed sample, allowing instrument performance monitoring, and aiding chromatographic alignment.

Instrument variability was determined by calculating the median relative standard deviation (RSD) for the standards that were added to each sample prior to injection into the mass spectrometers. Overall process variability was determined by calculating the median RSD for all endogenous metabolites (i.e., non-instrument standards) present in 100% of the pooled matrix samples. Experimental samples were randomized across the platform and run with QC samples spaced evenly.

For UPLC-MS/MS, all methods utilized a Waters ACQUITY ultra-performance liquid chromatography (UPLC) and a Thermo Scientific Q-Exactive high resolution/accurate mass spectrometer interfaced with a heated electrospray ionization (HESI-II) source and Orbitrap mass analyzer operated at 35,000 mass resolution. The sample extract was dried then reconstituted in solvents compatible to each of the four methods.

For data extraction and compound identification, raw data was extracted, peak-identified and QC processed using Metabolon's hardware and software. Compounds were identified by comparison to library entries of purified standards or recurrent unknown entities. Metabolon maintains a library based on authenticated standards that contains the retention time/index (RI), mass to charge ratio (*m/z*), and chromatographic data (including MS/MS spectral data) on all molecules present in the library. Furthermore, biochemical identifications were based on three criteria: retention index within a narrow RI window of the proposed identification, accurate mass match to the library ± 10 ppm, and the MS/MS forward and reverse scores between the experimental data and authentic standards.

RNA *in situ*-hybridization and spatial transcriptomics

To evaluate which cells are responsible for itaconate production, *Acod1* (Aconitate decarboxylase 1, also known as *Irg1*; Immunoresponsive gene 1), was measured using fluorescent RNAscope *in situ*-hybridization combined with immunohistochemistry. The *in situ*-hybridization was performed as previously described (all reagents purchased from Advanced Cell Diagnostics, Newark, CA, USA, unless stated

otherwise).¹¹ Briefly, formalin-fixed paraffin embedded (FFPE) slides were first deparaffinized, incubated with RNAscope hydrogen peroxide, and then boiled in RNAscope Target retrieval solution for 15 min. The dried sections were then treated with Proteinase IV for 30 min at room temperature (RT) and incubated with target probe (RNAscope Probe-Mm-Irg1, 450241) at 40°C for 2 hr, after which they were hybridized with RNAscope Multiplex FL v2 AMP for 30 min at 40°C. The HRP signal was developed by incubating the slides with RNAscope Multiplex FL v2 HRP for 15 min at 40°C, with Opal 570 dye (PN FP1488001KT, Akoya Biosciences, Marlborough, MA, USA) diluted in TSA for 30 min at 40°C and finally with RNAscope Multiplex FL v2 HRP blocker for 15 min at 40°C. After the hybridization the slides were blocked with 10% goat serum for 1 hour at RT and then incubated with anti-Iba1 (rabbit, 019-19714, Fujifilm Wako Chemicals, Richmond, VA, USA) and anti-GFAP (chicken, Alexa 647 conjugated) overnight at RT, both at 1:100 dilution in 3% goat serum and 0.2% Triton-X100 in 0.1 M PBS. After washing, the slides were incubated with secondary antibody Alexa Fluor goat-anti-rabbit 488 (1:400 dilution in 3% goat serum and 0.2% Triton-X100 in 0.1 M PBS) for 2 hr at RT and counterstained with DAPI.

Spatial transcriptomics was completed at NanoString Technologies (Seattle, WA, USA). After arrival, the FFPE mouse brain sections were baked for 1 hr at 65°C, after which they were processed on a Leica automation platform with a protocol that includes three major steps: 1) slide baking, 2) Antigen Retrieval for 20 min at 100°C, 3) 0.1 µg/ml Proteinase K treatment for 15 min. Slides were then incubated with GeoMx WTA assay probe cocktail overnight. On the following day the slides were washed and incubated with fluorescent anti-Tmem119 and anti-GFAP antibodies or anti-NeuN and anti-GFAP antibodies barcoded with photocleavable oligonucleotide tagged RNA probes (Figure 4(a) and (b)) before loading onto a Nanostring GeoMx Mouse Whole Transcriptome Atlas Digital Profiler. The slides were fluorescently scanned, and regions of interest (ROI) were selected (Figure 4(a) and (b)). The ROIs were segmented using the fluorescent antibodies so that the transcriptomes of Tmem119+ microglia, GFAP+ astrocytes, and NeuN+ neurons could be collected separately. Sequencing was completed on an Illumina NGS platform as previously described.¹²

Neurofilament light (NF-L) assay

To assess neurodegeneration, plasma samples were sent to PBL Assay Science (Piscataway, NJ, USA) and

analyzed using the Simoa™ NF-Light® kit (Cat #103186, Quanterix, Billerica, MA, USA).

Statistics

Median-scaled raw data was used to generate the heat maps in Figures 2 to 5 and Welch's two-sample *t*-test was used to test whether two unknown means were different between two independent populations. *Q*-values to estimate the false discovery rate are provided in Supplementary Table 2. The heat maps for Figure 6 were generated by using the negative normalized (mean + 1 SD) gene expression data from each cell type and brain area. To generate the bar graphs, significance was tested using a Brown-Forsythe and Welch's ANOVA test, followed by Dunnett's T3 multiple comparisons test (if there were more than two groups), as indicated in the figure legends. For principal component analysis, each principal component is a linear combination of every metabolite, and the principal components are uncorrelated. The first principal component was computed by determining the coefficients of the metabolites that maximized the variance of the linear combination. The second component finds the coefficients that maximize the variance with the condition that the second component is orthogonal to the first. Statistical analyses were performed using GraphPad Prism software 9.3.1 (GraphPad Software, LaJolla, CA, USA), and normality was assessed using the Kolmogorov–Smirnov test. Statistical tests and sample sizes are provided in each figure legend, and *p* values less than 0.05 were considered to be statistically significant. Statistically significant outliers, calculated using GraphPad Prism QuickCalcs, were excluded from the datasets. Data are presented as mean ± SD.

Results

Overview of the analysis

The timeline of the experiment is presented in Figure 1 (a). The infarct and equivalent area of the cortex from the contralateral hemisphere were dissected and removed for the metabolomic analysis at each time point. Infarcts were removed so that changes in metabolism in the surviving brain could be evaluated without the confound of hematogenous immune cells at the primary infarct site. The remaining ipsilateral hemisphere, and the equivalent region from the remaining contralateral hemisphere, were then dissected and used for the metabolomic evaluation (Figure 1(b)). Equivalent brain regions from young naïve mice, aged naïve mice, and sham mice were dissected and used for metabolomic analysis as reference controls.

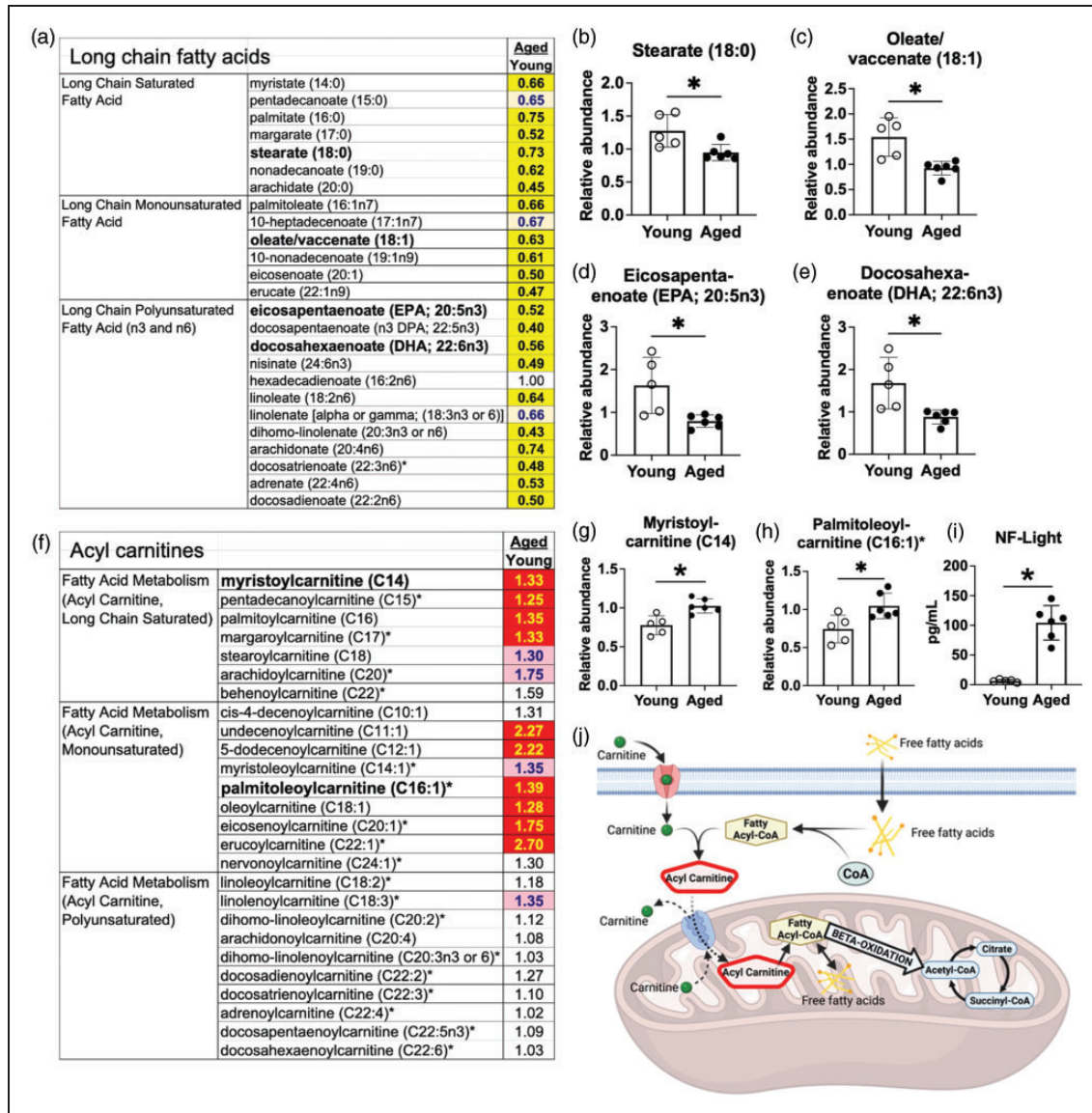


Figure 2. There is a reduction in long chain fatty acids and an increase in acyl carnitines in the aging brain. (a) Many long chain fatty acids were decreased in aged naïve mice compared to young naïve mice. (b–e) Representative long chain fatty acids: (b) Stearate (18:0) (c) Oleate/vaccenate (18:1) (d) Eicosapentaenoate (EPA; 20:5n3) (e) Docosahexaenoate (DHA; 22:6n3) (f) Some, but not all, species of the medium and long chain acyl carnitines were increased in aged naïve mice compared to young naïve mice. (g–h) Representative acyl carnitines: (g) Myristoylcarnitine (h) Palmitoleoylcarnitine. (i) Neurofilament Light (NF-Light) levels were increased in the plasma of the aged naïve mice compared to young naïve mice and (j) A schematic illustration of transportation of fatty acids into mitochondria before metabolism. After crossing the cell membrane, free fatty acids are conjugated with coenzyme-A (CoA) to form fatty acyl-CoAs, which are subsequently combined with carnitine. The resulting acyl carnitines can cross the mitochondrial membrane, after which carnitine is released, and the newly formed fatty acyl CoAs proceed to β -oxidation. Bar graphs: * $p < 0.05$ by unpaired two-tailed t test with Welch's correction, $n = 5-6$. Key for the heatmaps A&F: The numbers in the heatmaps indicate fold change with significance tested by Welch's two-sample t test. Yellow- and red-shaded cells indicate $p \leq 0.05$ (red indicates that the mean values are significantly higher, and yellow indicates that they are significantly lower). Light red- and light-yellow shaded cells indicate $0.05 < p < 0.10$.

The total number of biochemicals Detected by metabolomic analysis of each brain region was 707. At a significance level of $p < 0.05$ (5% of all detected metabolites), 35 differences between groups can be expected by random chance. Supplementary Table 1

shows the number of significantly different metabolites when the following comparisons were made: (1) young naïve mice compared to aged naïve mice, (2) stroked mice at each time point compared to aged naïve mice, (3) ipsilateral hemispheres compared to contralateral

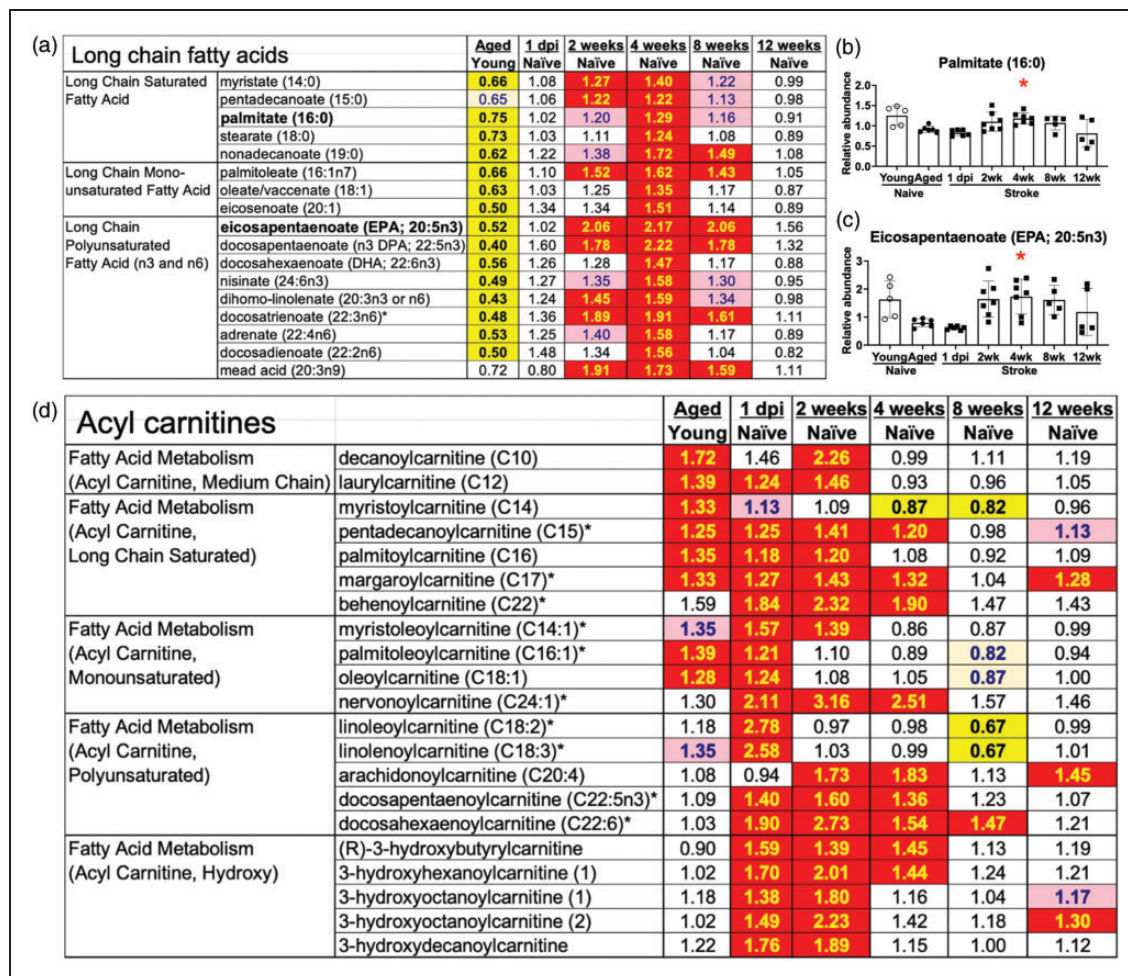


Figure 3. There is an increase in long chain fatty acids and acyl carnitines in the ipsilateral hemisphere for at least 4 weeks post stroke. (a) Long chain fatty acids peaked at 4 weeks after stroke. (b–c) Representative long chain fatty acids: (b) Palmitate (16:0), (c) Eicosapentaenoate (EPA; 20:5n3) and (d) Several acyl carnitines were already elevated at 1 day post ischemia. Bar graphs: * $p < 0.05$ by Brown-Forsythe and Welch's ANOVA test followed by Dunnett's T3 multiple comparisons test, all groups compared to the aged naïve group, $n = 5-7$. See Figure 2 legend for the key to the heatmaps in A&D.

hemispheres at matched time points, (4) stroked mice compared to sham mice at matched time points, (5) contralateral hemispheres at each time point compared to aged naïve mice, (6) sham mice at each time point compared to aged naïve mice, and 7) contralateral hemispheres compared to sham mice at matched time points. Supplementary Table 2 provides a full list of the metabolites changed with each comparison and Supplementary Table 3 provides a list of the metabolic pathways changed with each comparison. The data are also available at MetaboLights database (<https://www.ebi.ac.uk/metabolights>) where it can be found with the identifier MTBLS5543.

There were 190 statistically significant changes by Welch's two-sample t -test between the samples from the young and aged naïve mice, while there were 202 changes at 1 dpi when compared to aged naïve brains, 153 changes at 1 dpi when compared to time

point-matched contralateral hemispheres, and 167 changes at 1 dpi when compared to time point-matched samples from sham mice.

Although, depending on study design, tissue from naïve mice, sham mice and contralateral hemispheres from stroked mice are valid controls for preclinical stroke experiments, there were differences in the metabolic changes in the tissue taken from the aged naïve mice, sham mice, and contralateral hemispheres of the stroked mice. The data in Supplementary Table 2 provides a reference list of the changes for the sham mice and contralateral hemispheres of the stroked mice when compared to age-matched naïve mice and stroked mice. However, despite these differences, the overall pattern of metabolic changes caused by stroke was comparable regardless of which control was used (Supplementary Figure 1).

To provide an overview of the study, the difference between young and aged naïve mice was visualized

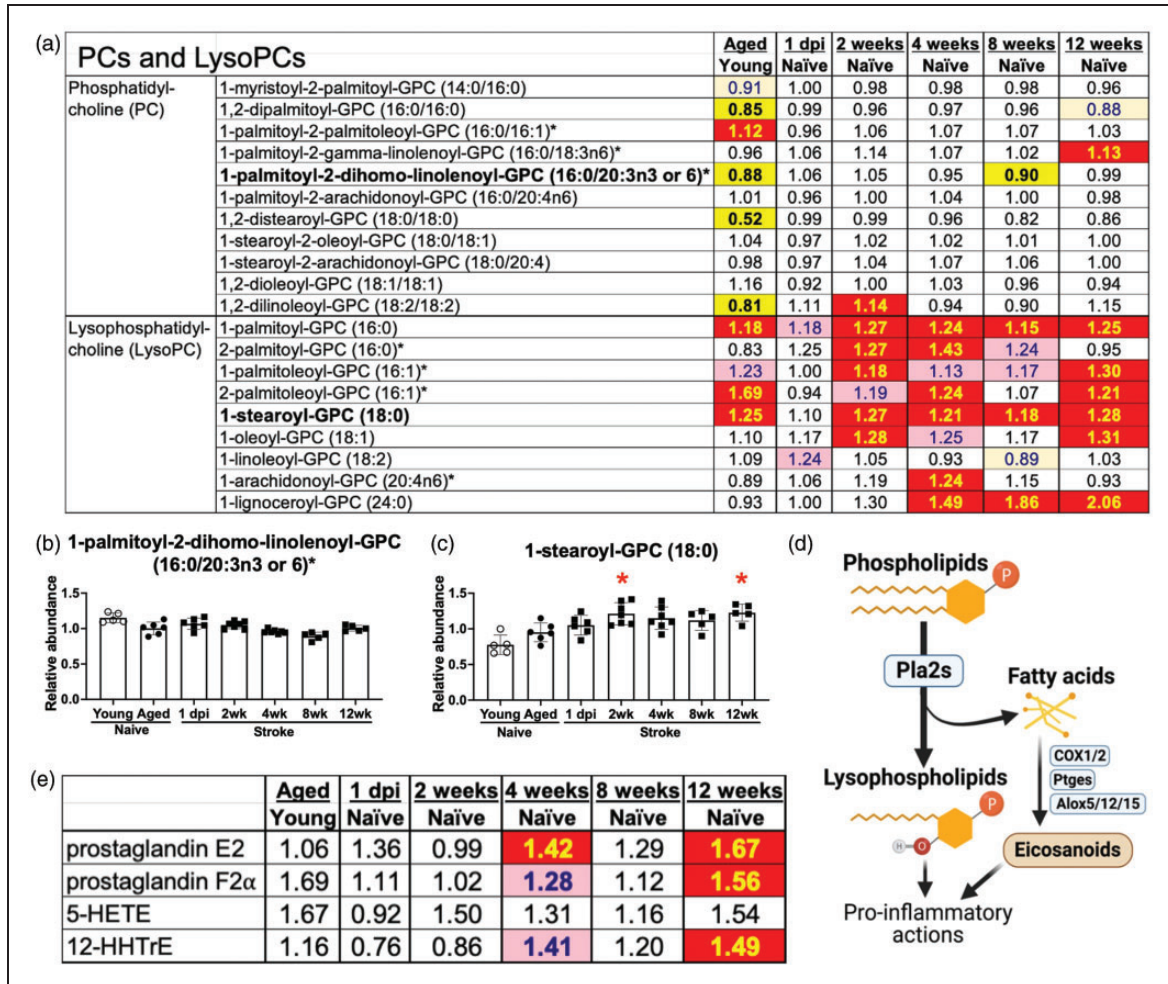


Figure 4. Lysophosphatidylcholines, but not phosphatidylcholines, were increased for 12 weeks after stroke. (a) Phosphatidylcholine levels were relatively unchanged in the weeks after stroke but lysophosphatidylcholine levels were increased for 12 weeks after stroke. (b) Representative phosphatidylcholine R1-palmitoyl-2-dihomo-linolenoyl-GPC (16:0/20:3n3 or 6). (c) Representative lysophosphatidylcholine 1-stearoyl-GPC (18:0). (d) Schematic illustration of the generation of lysophospholipids from phospholipids by Phospholipase A2s (Pla2s). Free fatty acids from this reaction can also be turned into eicosanoids by the actions of the enzymes cyclooxygenase 1 and 2 (Cox1/2), prostaglandin E₂ synthases (Ptges) and lipoxygenases (Alox5/12/15) and (e) Several eicosanoids were elevated at 4 and 12 weeks after stroke. Bar graphs: * $p < 0.05$ by Brown-Forsythe and Welch's ANOVA test followed by Dunnett's T3 multiple comparisons test, all groups compared to the aged naïve group, $n = 5-7$. See Figure 2 legend for the key to the heatmaps in A&E.

using principal component analysis (PCA) (Figure 1(c)). The PCA plot shows a clear separation of the young and aged mice along Principal Component 1. PCA comparing the aged naïve mice to the stroked mice showed distinct separation based on time point (Figure 1(d)). As expected, the samples collected at 1 dpi showed the most separation, with the later time points clustering progressively closer to the aged naïve controls.

Metabolic changes caused by aging

Of the 190 identified biochemicals that differed between the brains of young and aged naïve mice,

the most prominent alteration was a decrease in the levels of long chain fatty acids in the aged naïve mice (Figure 2(a)). As examples, there were reductions in stearate (18:0), oleate/vaccenate (18:1), eicosapentaenoate (EPA; 20:5n3), and docosahexaenoate (DHA; 22:6n3) in the brains of aged naïve mice compared with young naïve mice (Figures 2(b) to (e)). Multiple acyl carnitines were increased in the aged naïve brains (Figure 2(f)), with representative examples myristoylcarnitine (C14) and palmitoleoylcarnitine (C16:1) shown in Figures 2(g) and (h). This was associated with an increase in plasma neurofilament light levels (Figure 2(i)). The modification of fatty acids to

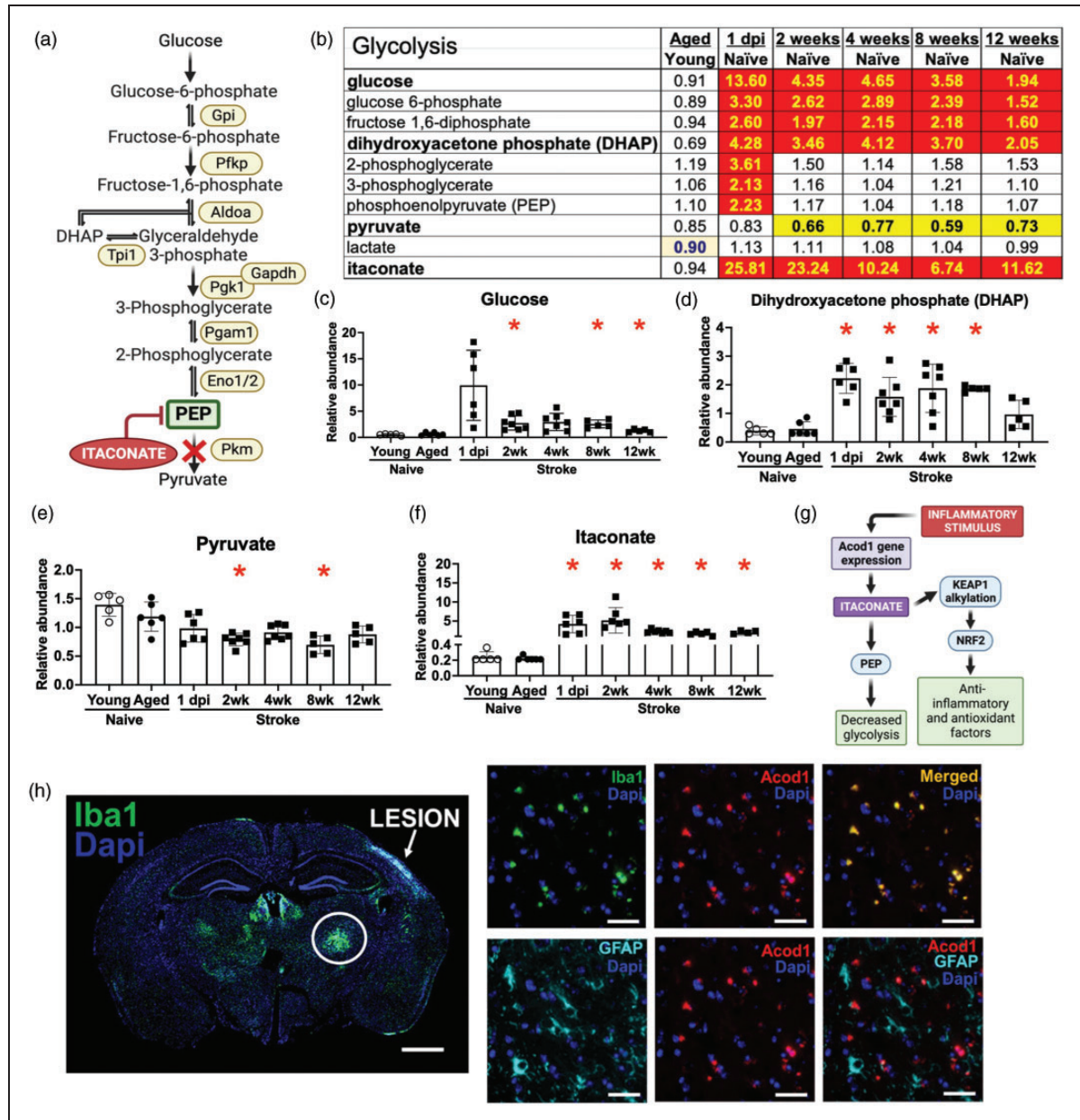


Figure 5. Stroke induces long-lasting alterations in glycolysis and itaconate production. (a) Glycolysis pathway with examples of associated genes. (b) Glycolysis is altered by stroke, and some of these modifications last for at least 12 weeks. Heatmap key provided in Figure 2 legend. (c–f) Graphs depicting the levels of representative compounds: (c) Glucose. (d) Dihydroxyacetone phosphate (DHAP). (e) Pyruvate. (f) Itaconate. * $p < 0.05$ by Brown-Forsythe and Welch's ANOVA test followed by Dunnett's T3 multiple comparisons test, all groups compared to aged naïve group, $n = 5-7$. (g) Itaconate, a competitive inhibitor of phosphoenolpyruvate (PEP), is produced by microglia and macrophages in response to an inflammatory signal that induces the expression of the *Acod1* gene. By alkylating Kelch-like ECH-associated protein 1 (KEAP1) and releasing nuclear factor erythroid 2-related factor 2 (Nrf2) to mediate its numerous anti-inflammatory and antioxidant effects, itaconate is also thought to defend against inflammation and oxidative stress. (h) Imaging of a whole brain section reveals that Iba1 immunoreactivity is highest in the ipsilateral thalamus, $n = 4$. Scale bar = 1000 μm . Higher magnification imaging reveals that the Iba1 positive cells also colocalize with *Acod1* RNA. There is little colocalization of GFAP with *Acod1* RNA, $n = 4$. Scale bars = 50 μm .

acyl carnitines is essential for transfer across the inner mitochondrial membrane and subsequent β -oxidation (Figure 2(j)). These data demonstrate that there is an increase in fatty acid metabolism in the aging mouse

brain and support previous data indicating that aging-induced mitochondrial dysfunction and neurodegeneration may activate mechanisms for the catabolism of myelin lipids.¹³

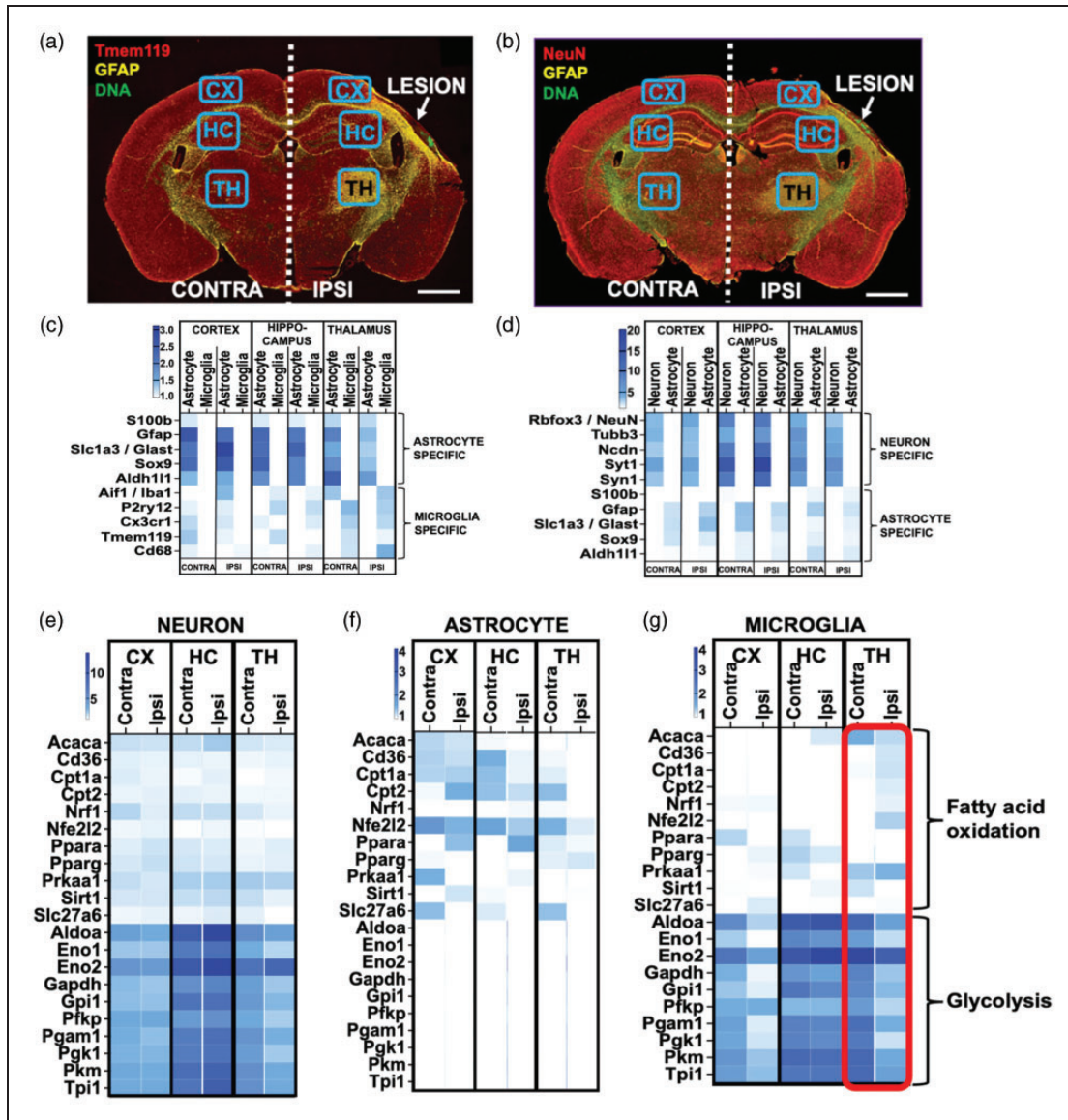


Figure 6. Changes in fatty acid oxidation and glycolysis localize to microglia in the ipsilateral thalamus. (a–b) For spatial transcriptomics, brain sections from aged mice at 4 weeks post stroke were stained with antibodies against Tmem119 and GFAP (a.), or NeuN and GFAP (b.). Gene expression data was gathered from cells expressing these markers from ipsilateral cortex (CX), hippocampus (HC) and thalamus (TH), and corresponding areas from the contralateral side, $n = 4$. Scale bars 1000 μm . (c–d) To confirm cell specificity the expression of genes that are traditionally associated with astrocytes and microglia (c.), and neurons and astrocytes (d.) was assessed in the transcripts isolated from each brain region using each marker and (e–g) The overall expression of genes related to glycolysis is higher in neurons and microglia than that of genes related to fatty acid oxidation, whereas astrocytes express more genes related to fatty acid oxidation than those related to glycolysis. With the exception of a modest decrease in glycolysis related genes in the ipsilateral thalamus, neuronal expression of these genes did not differ between the ipsi- and contralateral sides (e). In the ipsilateral hippocampus and thalamus, astrocytes reduced the expression of genes associated with fatty acid oxidation (f). Microglia in the ipsilateral cortex and thalamus displayed a marked reduction in the expression of genes linked to glycolysis, which was accompanied by an increase in genes related to fatty acid oxidation (shown in red rectangle) (g).

Metabolic changes caused by stroke

There was also a prominent alteration in the abundance of long chain fatty acids in the ipsilateral hemispheres of stroked mice compared to age-matched naïve controls. By 2 weeks after stroke, the levels of

multiple long chain fatty acids were significantly increased, peaking at 4 weeks after stroke; however, the levels were indistinguishable from naïve controls by 12 weeks after stroke (Figure 3(a) and representative compounds palmitate (16:0) and eicosapentaenoate (EPA; 20:5n3) in Figures 3(b) and (c)). In addition,

levels of acyl carnitines, such as pentadecanoylcarnitine (C15), oleoylcarnitine (C18:1), docosapentaenoylcarnitine (C22:5n3) or 3-hydroxyhexanoylcarnitine (1), were increased by stroke (Figure 3(d)); however, acyl carnitine levels were largely normalized by 8 weeks after stroke. These results indicate that there is an increase in the β -oxidation of fatty acids for at least 4 weeks in the ipsilateral hemisphere, which may be due to the catabolism of myelin lipid debris in areas of secondary neurodegeneration in the weeks after stroke.^{14,15}

Neurotoxic astrocytes secrete toxic phosphatidylcholines (PCs).¹⁶ Although there were few substantial changes in the expression levels of PCs (Figure 4(a) and (b)), aging raised several LysoPCs, and multiple LysoPCs were markedly higher for 12 weeks following stroke (Figure 4(a) and (c)). During inflammation, PCs are converted into LysoPCs by phospholipase A₂ enzymes (Figure 4(d)), suggesting that the increase in LysoPCs following stroke may be caused by chronic inflammation. Phospholipase A₂ also leads to the production of pro-inflammatory eicosanoids through the activity of other enzymes like cyclooxygenase 1 and 2 (Cox1 and Cox2), prostaglandin E₂ synthases (Ptges) and lipoxygenases (Alox5, Alox12 and Alox15).^{17,18} Several eicosanoids, including prostaglandin E₂, prostaglandin F₂ α , and 12-hydroxyheptadecatrienoic acid (12-HHTrE), were elevated at 4 and 12 weeks after stroke (Figure 4(e)).

Glucose levels were also increased in the ipsilateral hemispheres of aged mice after stroke, along with several other glycolysis pathway metabolites (Figure 5). However, rather than an increase in glycolysis, we interpret these alterations as the result of a blockage in glycolytic flux because pyruvate, the product of glycolysis, was decreased in the stroke tissue compared to the equivalent tissue from aged naïve mice (Figure 5(b) to (e)). At 1 dpi, an increase in phosphoenolpyruvate (PEP) corresponded with an increase in itaconate. Two weeks post stroke and thereafter, the reduction in pyruvate corresponded with increased dihydroxyacetone phosphate (DHAP) (Figure 5(b) and (d)). Notably, itaconate is an inhibitor of glycolysis as well as protective against inflammation and oxidative stress (Figure 5(g)).

To localize the increase in itaconate we performed RNAscope in situ-hybridization for *Acod1* combined with Iba1 immunostaining for microglia/macrophages and GFAP immunostaining for astrocytes. As shown in Figure 5(h), *Acod1* colocalized with Iba1+ cells in the ipsilateral thalamus area, with approximately 95% of the Iba1 positive cells in the ipsilateral thalamus colocalizing with *Acod1*, and 10–15% of the GFAP expressing cells colocalizing with *Acod1*.

To validate the observed alterations in fatty acid metabolism and glycolysis, and to further identify the brain areas and cell types responsible for these changes,

we conducted a spatial transcriptomic experiment with aged mice at 4 weeks post stroke. Tissue sections were stained with antibodies against Tmem119 for microglia, GFAP for astrocytes and NeuN for neurons (Figure 6(a) and (b)), and cell type specific RNA was collected from cortex, hippocampus, and thalamus from both ipsi- and contralateral hemispheres. Cell enrichment for the RNA isolated using each barcoded antibody was confirmed by measuring expression levels of genes associated with astrocytes and microglia (Figure 6(c)), and astrocytes and neurons (Figure 6(d)) for each RNA pool from each brain area.

In the neurons, genes associated with glycolysis were more highly expressed than genes associated with fatty acid oxidation and there were no major changes in the ipsilateral versus contralateral hemisphere (Figure 5(e)). In astrocytes, genes associated with fatty acid oxidation were more highly expressed than genes associated with glycolysis, and the strongest change was a decrease in the expression of genes related to fatty acid oxidation in the ipsilateral thalamus (Figure 6(f)). In microglia, genes associated with glycolysis were more highly expressed than genes associated with beta oxidation. However, in the ipsilateral thalamus there was a pronounced increase in the expression of beta oxidation associated genes, and a corresponding decrease in the expression of genes related to glycolysis (Figure 6(g)).

Regarding neurotransmitters, stroke decreased the levels of glutamate, dopamine, serotonin, and adenosine in the ipsilateral hemispheres of the aged mice, with the reductions in glutamate, dopamine, and adenosine persisting for 8–12 weeks (Figure 7(a) to (d)). The reduction in neurotransmitters after stroke occurred in conjunction with an increase in neurofilament light in the plasma at 1 day and 2 weeks after stroke (Figure 7(e)). Figure 7(f) provides a summary of the main findings from this study.

Discussion

The brain is highly reliant on glucose for energetic requirements. Although fatty acid oxidation does occur within the brain, it is slower and consumes more oxygen than ATP generation from glucose and exposes neural cells to more oxidative stress.¹⁹ Little is currently known about how metabolism changes with aging in the rodent brain despite many factors likely contributing to age-dependent changes in brain metabolism. For example, changes in the blood-brain barrier (BBB)²⁰ may result in the accumulation of plasma proteins, which can cause inflammation and interfere with neuronal circuitry.²¹ Additionally, alterations in mitochondrial structure and function have been recognized as a hallmark of the aging brain^{22,23} and

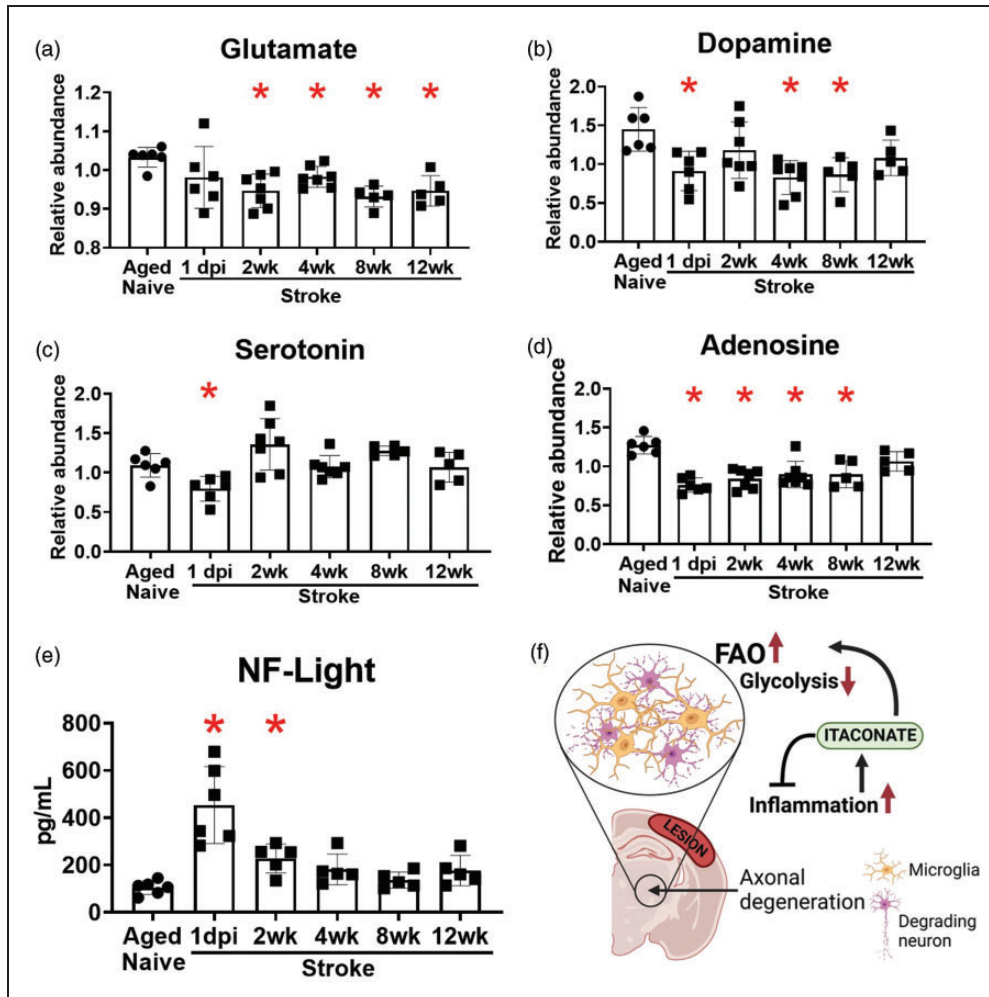


Figure 7. Levels of glutamate, dopamine, and adenosine were reduced for at least 8 weeks after stroke, and neurofilament light levels in the plasma were increased for 2 weeks after stroke. Graphical illustrations of the levels of glutamate (a), dopamine (b), serotonin (c) and adenosine (d) in the brain, and neurofilament light (e) in the plasma following the ischemic insult. * $p < 0.05$ by Brown-Forsythe and Welch's ANOVA test, followed by Dunnett's T3 multiple comparisons test, all groups compared to aged naive group, $n = 5-7$ and (f) Schematic illustration summarizing our findings. At locations where axonal degeneration occurs in the ipsilateral thalamus, microglia process neuronal debris. The inflammatory environment stimulates itaconate production, which helps to regulate inflammation and encourages enhanced fatty acid oxidation and decreased glycolysis in microglia.

neurotransmitters, such as dopamine and serotonin, decline with aging.^{24,25}

In this study, we observed an increase in the neurodegeneration biomarker neurofilament light (Nfl) in the plasma of mice between 7 and 18–20 months, and that this occurred in conjunction with a reduction in levels of long chain fatty acids and an increase in levels of acyl carnitines in the brain. The reduction in long chain fatty acids may be due to an age-related decline in white matter,²⁶ and the increase in acyl carnitines may be due to the catabolism of white matter debris at sites of age-related neurodegeneration. This is because long chain fatty acids destined for oxidation are conjugated to carnitine by Cpt1a residing in the outer mitochondrial membrane, which results in the

release of coenzyme A (CoA). The resulting acyl carnitines are then transported across the intermembrane space by carnitine/acylcarnitine translocase and acted upon by the inner membrane Cpt2, which releases carnitine and reconstitutes the long chain fatty acid with CoA for mitochondrial fatty acid β -oxidation. While this provides an alternative source of acetyl-CoA to maintain cellular bioenergetics it also provides a method for catabolizing excess fatty acids derived from myelin breakdown.^{27,28} This opens the possibility that radiopharmaceutical imaging probes that detect fatty acid oxidation could be used to image and localize age-related neurodegeneration.

The metabolic alterations that take place in the brain during the recovery phase following stroke are

also largely unexplored. To our knowledge, existing studies have been restricted to the brains of young rodents and only at acute (1–3 days), and sub-acute (7 days) time points post stroke.^{29–33} Age is the largest non-modifiable risk factor for ischemic stroke,¹ and metabolic changes in the aging brain may make it more vulnerable to the aftereffects of stroke. Therefore, in this study, we also evaluated the metabolic changes that occur in the brain in aged mice at acute, sub-acute, and chronic time points.

We found that long chain fatty acids were elevated between 2 and 8 weeks after stroke. Unlike with aging, where there is slow progressive loss of white matter, this alteration may be due to the sudden release and subsequent breakdown of a large quantity of myelin debris generated by stroke. We have previously shown that there is a similar accumulation of cholesterol crystals, sphingomyelins, sulfatides, and lipid droplets due to the breakdown of myelin after stroke.^{14,15} Alongside the increase in fatty acid levels, we found that there was an increase in acyl carnitine levels. Like aging, this hallmark of increased fatty acid metabolism may be due to the catabolism of white matter debris, although generated by stroke rather than age-related neurodegeneration. Spatial transcriptomics localized these changes to TMEM119 positive cells in the thalamus, which is the primary area of axonal degeneration in the DMCAO model of stroke. TMEM119 is a microglial marker not expressed by macrophages or other immune cells,^{34–37} thereby localizing these changes to microglia in degenerating white matter after stroke.

We also found that LysoPCs were elevated for 12 weeks after stroke. High levels of LysoPCs resulting from PC degradation have been associated with mitochondrial dysfunction and inflammation after ischemia.^{27,28} Recently, a group led by S. Liddelow¹⁶ reported that neurotoxic reactive astrocytes, induced by the secretion of $\text{IL-1}\alpha$, tumor necrosis factor alpha (TNF- α), and C1q by activated microglia,³⁸ induce cell death via the release of PCs. Fatty acids act as important secondary messengers in cell signaling, but they can also have pro-inflammatory effects,³⁹ and the accumulation of fatty acids in the brain has been associated with several neurodegenerative disorders.⁴⁰ Therefore, neurotoxic reactive astrocytes in the peri-infarct region could also be the source of these lipids. Future studies are necessary to determine the source of the increase in LysoPCs.

Our results also revealed that many glycolysis-related metabolites were upregulated at 1 day after stroke and were still elevated at 12 weeks. Concurrently, pyruvate was decreased, and itaconate, a glycolysis inhibitor, was found to be increased. RNA in situ hybridization for *Acod1*, which codes for the mitochondrial enzyme that produces itaconate, localized this increase to microglia

in the thalamus. Itaconate has been proposed to disrupt glycolysis at the level of pyruvate kinase via competitive inhibition due to its structural similarity to PEP.⁴¹ Notably, the increase in PEP may be another level of regulation, as PEP is a competitive inhibitor of the enzyme triosephosphate isomerase (TPI), which converts DHAP into glyceraldehyde 3-phosphate. In support of this possibility, DHAP levels were increased for 12 weeks after stroke.⁴² Therefore, glycolysis may initially be inhibited after stroke at the level of pyruvate kinase via the accumulation of itaconate and then at the level of TPI via the accumulation of PEP. These data indicate that glycolytic flow is impaired for at least 12 weeks after stroke and suggest that itaconate is an early regulator of this alteration in metabolic homeostasis. They also localize much of this change to microglia in degenerating white matter.

Itaconate is a metabolite discovered in 1840 by Gustav Crasso.⁴³ However, its role in regulating inflammation was unclear until 2011, when it was first reported to play a role in mammalian immune responses.^{44–46} Itaconate is produced in microglia and macrophages by the action of the highly inducible *Acod1* gene when phagocytes respond to an inflammatory stimulus, such as an infection or injury. The enzyme produced by *Acod1* catalyzes the production of itaconate from the TCA cycle metabolites citrate and cis-aconitate. Importantly, the induction of itaconate can protect against oxidative stress and is anti-inflammatory via the alkylation of kelch-like ECH-associated protein 1 (KEAP1).⁴⁷ Under normal conditions, KEAP1 exists to inhibit nuclear factor erythroid 2-related factor 2 (Nrf2) in the cytoplasm; however, alkylation of KEAP1 leads to accumulation of Nrf2, resulting in multiple antioxidant and anti-inflammatory actions that may be important for stroke recovery (Figure 5(g)).^{48,49}

Metabolic switching in immune cells is an important mechanism that enables them to change their metabolism as they respond to and interact with their environment. These changes can involve the upregulation or downregulation of various metabolic pathways, such as glycolysis, fatty acid metabolism, and oxidative phosphorylation. For example, during times of high demand, such as when the immune system is responding to an infection, immune cells may increase their reliance on glycolysis. On the other hand, during times of low demand, such as when the immune system is in a resting state, immune cells may rely more on oxidative phosphorylation.⁵⁰ The data provided here support that a switch from glucose to fatty acid metabolism in microglia after stroke may reflect their processing of lipid debris derived from the breakdown of myelin.

This study has several limitations, including the possibility that some of the changes we report are due to the post-mortem interval between perfusion and tissue dissection and the freezing of the tissue.⁵¹ However, tissue processing was the same for each group and so postmortem changes are likely to be consistent between groups. Therefore, the changes we report in brain metabolism between groups are unlikely to be artifactual changes that occurred during tissue dissection. This study was also only completed in C57BL/6J male mice using a single stroke model. Validation of the key findings is necessary using females and additional models. Additionally, inflammation, gliosis, and immune cell infiltration into the ipsilateral hemisphere results in an increase in microglia, astrocytes, and peripheral immune cells compared to control tissues. This difference in cellular composition of the ipsilateral hemisphere almost certainly contributes to the metabolic differences reported. Relatedly, although the spatial transcriptomics revealed that the metabolic changes at 4 weeks are likely due to the microglial response to axonal degeneration in the thalamus, the metabolic differences we identified at the other timepoints may include changes in other cell types in other brain regions. Also, because we focused our study on the recovering brain rather than the infarct, the metabolic changes that occur in the infarct after stroke still need to be delineated. Nevertheless, to the best of our knowledge, this investigation is the first global characterization of the metabolic profile of the aging mouse brain during the first 12 weeks of recovery following ischemic stroke, and it provides novel insight into the changes in metabolic homeostasis that occur in the brain during recovery. The results provide a foundation for future studies focused on determining the underlying functions of these changes in metabolic homeostasis.

In conclusion, this study has revealed that stroke alters glycolysis and lipid metabolism in the brain for at least 12 weeks, that these changes predominantly localize to microglia in areas of degenerating white matter, and that itaconate may be a central regulator of both this metabolic switch as well as the inflammatory response in degenerating white matter (Figure 7 (f)). Additional research is necessary to determine the precise role of itaconate as well as the extent to which the changes reflect mitochondrial dysfunction in microglia due to tissue damage, versus an adaptation to altered fuel abundance due to the presence of myelin lipid debris. Nevertheless, an exciting implication of these results is that while elevated levels of neurofilament light in plasma are a useful marker of neurodegeneration, metabolic imaging for changes in beta oxidation and glycolysis could potentially be used as a method for pinpointing where in the brain

neurodegeneration is taking place and for monitoring treatments.

Funding

The author(s) disclosed receipt of the following financial support for the research, authorship, and/or publication of this article: This work was funded by NINDS R01NS096091 (KPD), NIA R01AG063808 (KPD), United States Department of Veterans Affairs I01RX003224 (RGS), and the Leducq Foundation Transatlantic Network of Excellence Stroke-IMPACT (KPD).

Acknowledgements

We are grateful to Metabolon Inc. for their expertise and assistance throughout all aspects of our study. Schematics created with BioRender.com.



Declaration of conflicting interests

The author(s) declared no potential conflicts of interest with respect to the research, authorship, and/or publication of this article.

Authors' contributions

SL, MTG, BKM, KEJ, TVN and KD conducted the research, SL, DB, KD, and RS wrote the manuscript.

ORCID iDs

Sanna H Loppi  <https://orcid.org/0000-0002-8848-0453>
Danielle A Becktel  <https://orcid.org/0000-0002-8463-0282>

Supplemental material

Supplemental material for this article is available online.

References

- Boehme AK, Esenwa C and Elkind MSV. Stroke risk factors, genetics, and prevention. *Circ Res* 2017; 120: 472–495.
- Jovin TG, Chamorro A, Cobo E, et al. Thrombectomy within 8 hours after symptom onset in ischemic stroke. *N Engl J Med* 2015; 372: 2296–2306.
- de Los Ríos la Rosa F, Khoury J, Kissela BM, et al. Eligibility for intravenous recombinant tissue-type plasminogen activator within a population: the effect of the European Cooperative Acute Stroke Study (ECASS) III trial. *Stroke* 2012; 43: 1591–1595.
- Sun L, Yang X, Yuan Z, et al. Metabolic reprogramming in immune response and tissue inflammation. *ATVB* 2020; 40: 1990–2001.
- Krakauer JW, Carmichael ST, Corbett D, et al. Getting neurorehabilitation right: what can be learned from animal models? *Neurorehabil Neural Repair* 2012; 26: 923–931.
- Yousufuddin M and Young N. Aging and ischemic stroke. *Aging (Albany NY)* 2019; 11: 2542–2544.
- Faul F, Erdfelder E, Lang A-G, et al. G*power 3: a flexible statistical power analysis program for the social,

- behavioral and biomedical sciences. *Behav Res Methods* 2007; 39: 175–191.
8. Lapchak PA, Zhang JH and Noble-Haesslein LJ. RIGOR guidelines: escalating STAIR and STEPS for effective translational research. *Transl Stroke Res* 2013; 4: 279–285.
 9. Percie Du Sert N, Hurst V, Ahluwalia A, et al. The ARRIVE guidelines 2.0: updated guidelines for reporting animal research. *PLoS Biol* 2020; 18: e3000410–e3000410.
 10. Doyle KP, Fathali N, Siddiqui MR, et al. Distal hypoxic stroke: a new mouse model of stroke with high throughput, low variability and a quantifiable functional deficit. *J Neurosci Methods* 2012; 207: 31–40.
 11. Wang F, Flanagan J, Su N, et al. RNAscope. *J Mol Diagn* 2012; 14: 22–29.
 12. Zollinger DR, Lingle SE, Sorg K, et al. GeoMx™ RNA assay: high multiplex, digital, spatial analysis of RNA in FFPE tissue. *Methods Mol Biol* 2020; 2148: 331–345.
 13. Klosinski LP, Yao J, Yin F, et al. White matter lipids as a ketogenic fuel supply in aging female brain: implications in Alzheimer's disease. *EBioMedicine* 2015; 2: 1888–1904.
 14. Becktel DA, Zbesko JC, Frye JB, et al. Repeated administration of 2-hydroxypropyl- β -cyclodextrin (HP β CD) attenuates the chronic inflammatory response to experimental stroke. *J Neurosci* 2022; 42: 325–348.
 15. Chung AG, Frye JB, Zbesko JC, et al. Liquefaction of the brain following stroke shares a similar molecular and morphological profile with atherosclerosis and mediates secondary neurodegeneration in an osteopontin-dependent mechanism. *eNeuro* 2018; 5: ENEURO.0076-18.2018.
 16. Guttenplan KA, Weigel MK, Prakash P, et al. Neurotoxic reactive astrocytes induce cell death via saturated lipids. *Nature* 2021; 599: 102–107.
 17. Dennis EA. Phospholipase A2 in eicosanoid generation. *Am J Respir Crit Care Med* 2000; 161: S32–S35.
 18. Bingham IIC and Austen KF. Phospholipase A2 enzymes in eicosanoid generation. *Proc Assoc Am Physicians* 1999; 111: 516–524.
 19. Schönfeld P and Reiser G. Why does brain metabolism not favor burning of fatty acids to provide energy? Reflections on disadvantages of the use of free fatty acids as fuel for brain. *J Cereb Blood Flow Metab* 2013; 33: 1493–1499.
 20. Banks WA, Reed MJ, Logsdon AF, et al. Healthy aging and the blood-brain barrier. *Nat Aging* 2021; 1: 243–254.
 21. Zlokovic BV. Neurovascular pathways to neurodegeneration in Alzheimer's disease and other disorders. *Nat Rev Neurosci* 2011; 12: 723–738.
 22. Stahon KE, Bastian C, Griffith S, et al. Age-related changes in axonal and mitochondrial ultrastructure and function in white matter. *J Neurosci* 2016; 36: 9990–10001.
 23. Yin F, Sancheti H, Patil I, et al. Energy metabolism and inflammation in brain aging and Alzheimer's disease. *Free Radic Biol Med* 2016; 100: 108–122.
 24. Morgan DG, May PC and Finch CE. Dopamine and serotonin systems in human and rodent brain: effects of age and neurodegenerative disease. *J Am Geriatr Soc* 1987; 35: 334–345.
 25. Morgan D. The dopamine and serotonin systems during aging in human and rodent brain. A brief review. *Prog Neuropsychopharmacol Biol Psychiatry* 1987; 11: 153–157.
 26. Gunning-Dixon FM, Brickman AM, Cheng JC, et al. Aging of cerebral white matter: a review of MRI findings. *Int J Geriatr Psychiatry* 2009; 24: 109–117.
 27. Jin R, Yang G and Li G. Inflammatory mechanisms in ischemic stroke: role of inflammatory cells. *J Leukoc Biol* 2010; 87: 779–789.
 28. Rutkowsky JM, Knotts TA, Ono-Moore KD, et al. Acylcarnitines activate proinflammatory signaling pathways. *Am J Physiol Endocrinol Metab* 2014; 306: E1378–E1387.
 29. Hsu WH, Shen YC, Shiao YJ, et al. Combined proteomic and metabolomic analyses of cerebrospinal fluid from mice with ischemic stroke reveals the effects of a Buyang Huanwu decoction in neurodegenerative disease. *PLoS One* 2019; 14: e0209184.
 30. Tanaka E, Ogawa Y, Fujii R, et al. Metabolomic analysis and mass spectrometry imaging after neonatal stroke and cell therapies in mouse brains. *Sci Rep* 2020; 10: 21881.
 31. Loppi S, Kolosowska N, Kärkkäinen O, et al. HX600, a synthetic agonist for RXR-Nurr1 heterodimer complex, prevents ischemia-induced neuronal damage. *Brain Behav Immun* 2018; 73: 670–681.
 32. Huang Q, Li C, Xia N, et al. Neurochemical changes in unilateral cerebral hemisphere during the subacute stage of focal cerebral ischemia-reperfusion in rats: an ex vivo 1H magnetic resonance spectroscopy study. *Brain Res* 2018; 1684: 67–74.
 33. Feng S-Q, Aa N, Geng J-L, et al. Pharmacokinetic and metabolomic analyses of the neuroprotective effects of salvianolic acid a in a rat ischemic stroke model. *Acta Pharmacol Sin* 2017; 38: 1435–1444.
 34. Bennett ML, Bennett FC, Liddel SA, et al. New tools for studying microglia in the mouse and human CNS. *Proc Natl Acad Sci U S A* 2016; 113: E1738–E1746.
 35. Kaiser T and Feng G. Tmem119-EGFP and Tmem119-creERT2 transgenic mice for labeling and manipulating microglia. *eNeuro* 2019; 6: ENEURO.0448-18.2019.
 36. Ruan C, Sun L, Kroshilina A, et al. A novel Tmem119-tdTomato reporter mouse model for studying microglia in the central nervous system. *Brain Behav Immun* 2020; 83: 180–191.
 37. Satoh J, Ichi Kino Y, Asahina N, et al. TMEM119 marks a subset of microglia in the human brain. *Neuropathology* 2016; 36: 39–49.
 38. Liddel SA, Guttenplan KA, Clarke LE, et al. Neurotoxic reactive astrocytes are induced by activated microglia. *Nature* 2017; 541: 481–487.
 39. Romano A, Koczwara JB, Gallelli CA, et al. Fats for thoughts: an update on brain fatty acid metabolism. *Int J Biochem Cell Biol* 2017; 84: 40–45.
 40. Schönfeld P and Reiser G. How the brain fights fatty acids' toxicity. *Neurochem Int* 2021; 148: 105050.
 41. Sakai A, Kusumoto A, Kiso Y, et al. Itaconate reduces visceral fat by inhibiting fructose 2,6-bisphosphate synthesis in rat liver. *Nutrition* 2004; 20: 997–1002.

42. Grüning N-M, Du D, Keller MA, et al. Inhibition of triosephosphate isomerase by phosphoenolpyruvate in the feedback-regulation of glycolysis. *Open Biol* 2014; 4: 130232.
43. Crasso GL. Untersuchungen über das Verhalten der Citronensäure in höherer Temperatur und die daraus hervorgehenden Produkte. *Ann Chem Pharm* 1840; 34: 53–84.
44. Sugimoto M, Sakagami H, Yokote Y, et al. Non-targeted metabolite profiling in activated macrophage secretion. *Metabolomics* 2012; 8: 624–633.
45. Strelko CL, Lu W, Dufort FJ, et al. Itaconic acid is a mammalian metabolite induced during macrophage activation. *J Am Chem Soc* 2011; 133: 16386–16389.
46. Shin J-H, Yang J-Y, Jeon B-Y, et al. ¹H NMR-based metabolomic profiling in mice infected with *Mycobacterium tuberculosis*. *J Proteome Res* 2011; 10: 2238–2247.
47. Mills EL, Ryan DG, Prag HA, et al. Itaconate is an anti-inflammatory metabolite that activates Nrf2 via alkylation of KEAP1. *Nature* 2018; 556: 113–117.
48. Kobayashi EH, Suzuki T, Funayama R, et al. Nrf2 suppresses macrophage inflammatory response by blocking proinflammatory cytokine transcription. *Nat Commun* 2016; 7: 11624.
49. Tocmo R and Parkin K. S-1-propenylmercaptocysteine protects murine hepatocytes against oxidative stress via persulfidation of Keap1 and activation of Nrf2. *Free Radic Biol Med* 2019; 143: 164–175.
50. Ganeshan K and Chawla A. Metabolic regulation of immune responses. *Annu Rev Immunol* 2014; 32: 609–634.
51. Lowry OH, Passonneau JV, Hasselberger FX, et al. Effect of ischemia on known substrates and cofactors of the glycolytic pathway in brain. *J Biol Chem* 1964; 239: 18–30.